

Article

Comparative Investigation of the Undercooling Capacity and Single-Crystal Castability of Some Ni-Based Superalloys

Dexin Ma ^{1,2,*}, Yunxing Zhao ^{1,2}, Weitai Xu ¹, Fuze Xu ^{1,2}, Jianhui Wei ^{1,2} and Haijie Zhang ³ ¹ Shenzhen Wedge Central South Research Institute Co., Ltd., Shenzhen 518045, China² Powder Metallurgy Research Institute, Central South University, Changsha 410083, China³ Department of Metallurgy, University of Leoben, A-8700 Leoben, Austria

* Correspondence: madexin@csu.edu.cn

Abstract: The undercooling capacity of a superalloy is an essential physical property to determine its single-crystal (SC) castability, because stray grains (SGs) will be formed if the geometrical undercooling established at the platform extremities exceeds the undercooling capacity of the applied alloy. In the present work, both the undercooling capacity of eight Ni-based superalloys and their SC castability were experimentally investigated. The liquidus temperature, the critical temperature for grain nucleation, and hence the undercooling capacities of the investigated alloys were evaluated based on the temperature evolution during the heating and cooling processes. The current experimental study revealed a significant difference in undercooling capacity for the superalloys. In the production of SC blade castings, the tendency to form SG defects was found to be highly related to the alloy's undercooling capacity. The alloys having a low undercooling capacity of around 10 K were very prone to the formation of SGs. In comparison, the alloys with a moderate undercooling capacity from 20 K to 30 K could be easily cast into SC blades without SGs, exhibiting the best SC castability. Other factors influencing the SG formation were also analyzed. As a result, a criterion for the formation of geometry-related SG defects was proposed, in which the influence of the alloy undercooling capacity, casting geometry, and solidification condition are involved.



Citation: Ma, D.; Zhao, Y.; Xu, W.; Xu, F.; Wei, J.; Zhang, H. Comparative Investigation of the Undercooling Capacity and Single-Crystal Castability of Some Ni-Based Superalloys. *Crystals* **2023**, *13*, 57. <https://doi.org/10.3390/cryst13010057>

Academic Editor: Heinz-Günter Brokmeier

Received: 2 December 2022

Revised: 18 December 2022

Accepted: 21 December 2022

Published: 28 December 2022



Copyright: © 2022 by the authors. Licensee MDPI, Basel, Switzerland. This article is an open access article distributed under the terms and conditions of the Creative Commons Attribution (CC BY) license (<https://creativecommons.org/licenses/by/4.0/>).

Keywords: superalloy; single crystal; blade casting; undercooling capacity; stray grain

1. Introduction

The single-crystal (SC) structure of superalloy turbine blades can maximally enhance the efficiency of aero-engines compared to that with equiaxed grains or directional solidified structures. Because the grain boundaries are totally eliminated, the SC blades exhibit significantly better high-temperature performance such that the inlet temperature of the aero-engines can be increased. In the production of SC blade castings, the most critical problem is to establish an SC structure free of stray grains [1–5].

The formation of the SGs is one of the most common solidification defects in SC blade castings. This solidification defect is unacceptable because of the high-angle grain boundaries between the randomly orientated SGs. The SC castings are normally produced in a Bridgman-type vacuum furnace to ensure a sharp temperature gradient for directional solidification. The SGs are mostly formed at the platform extremities of the blade castings, where the alloy melt undergoes a relatively quick cooling rate [6–9]. When the local geometrical undercooling at the extremities exceeds the undercooling capacity of the utilized alloy, the nucleation of new grains occurs, resulting in the formation of the so-called geometry-induced SGs [10–14].

According to the state-of-the-art on the formation of SGs, many efforts have been focused on the influence of the solidification conditions of the SC castings [14–20]. In comparison, the effect of the undercooling ability of a superalloy on the formation of SGs has not been studied systematically. The undercooling capacity of an alloy refers to the

ability of the alloy to remain in liquid state without nucleation when the melt temperature drops below its liquidus line. In our previous studies [21–23], it was found that different superalloys have different undercooling capacities and different tendencies to form SGs. In the current work, eight Ni-based superalloys were selected to determine their undercooling capacities under the same process conditions. Then, the selected alloys were used to produce turbine blades in an industrial Bridgman furnace to investigate their SC castability in dependence on their undercooling capacity.

2. Experimental Section

2.1. Materials

Eight commercial Ni-based superalloys were selected to investigate their undercooling capacities. The chemical composition of the superalloys is summarized in Table 1. The alloys were also used to produce SC blade castings under industrial conditions to investigate their SC castability comparatively.

Table 1. Composition of the eight selected Ni-based superalloys (wt%).

Alloy	Alloying Element									
	Cr	Co	W	Mo	Al	Ti	Ta	Re	Hf	Total ($\sum C_i$)
CMSX-6	10.0	5.0	-	3.0	4.8	4.7	2.0	-	0.1	29.6
WZ30	3.5	6.0	6.5	0.4	5.8	0.15	8.0	4.95	0.03	35.33
MAR M247	8.2	9.2	9.5	0.5	5.6	0.7	3.2	-	1.05	37.95
CMSX-4	6.5	9.0	6.0	0.6	5.6	1.0	6.5	3.0	0.1	38.3
PWA1483	11.98	8.7	3.83	1.81	3.63	3.99	5.09	-	0.01	39.04
DZ445	13.15	10.0	4.50	1.76	4.13	2.30	4.75	-	-	40.59
DD483	12.18	9.23	3.89	1.85	3.53	4.00	4.98	-	0.01	39.67
IN939	22.4	19.0	2.0	-	1.9	3.7	1.4	-	-	50.4

2.2. Undercooling Experiment

In order to investigate the undercooling capacity of the selected Ni-based superalloys, casting clusters with small spherical sample overhangs were designed to measure the undercooling behavior of the superalloy during the solidification process. To obtain more measurement data, four wax samples of 12 mm in diameter were obtained in one wax pattern cluster, as illustrated in Figure 1a. The corresponding mold clusters were manufactured (Figure 1b). As shown in Figure 1c, two or three separated segments were used in each experiment, so that two or three alloys could be measured simultaneously but individually under the same process condition. An example of the as-solidified sample cluster is shown in Figure 1d.

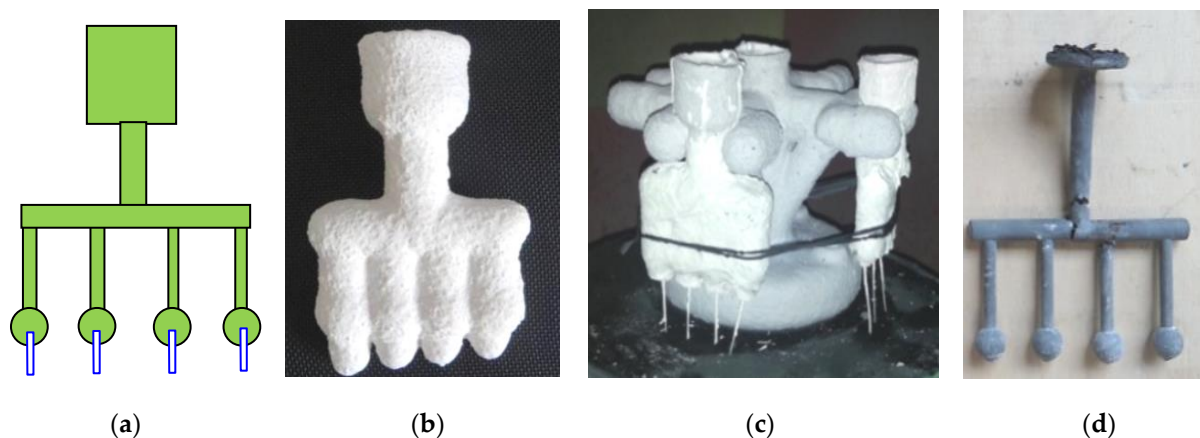


Figure 1. (a) Wax pattern cluster; (b,c) the corresponding shell mold and assembly; (d) solidified samples after experiment.

The ceramic molds of Al_2O_3 were prepared via a standard lost-wax procedure. The thermocouples in the ceramic sheaths were installed into the cavity center of the spherical molds to record the temperature evolution in the alloy samples during the undercooling experiments. During the preheating process in the vacuum furnace, the superalloy ingots pre-placed in the pouring cups were melted and poured into the individual mold cavities for the subsequent undercooling experiments. After a period of homogenization, the heaters were switched off to cool down the melt, followed by the gradual solidification of the superalloy. When the furnace temperature dropped to $1200\text{ }^\circ\text{C}$, the heaters were switched on again to start a new melting–solidification (heating–cooling) cycle, thus making it possible to obtain a new set of experimental data. During the periodic heating–cooling processes, namely the melting–solidification cycles, the temperature evolution of the samples was recorded to evaluate the critical nucleation undercooling of the superalloys.

2.3. Casting Experiment of SC Blades

In these experiments, the turbine blades, as characterized by abrupt profile (cross-section) variation at the transition from the aerofoil to the platform, were manufactured. Blades with this geometrical feature are the main components of aero-engines. The extremities of the platforms are very sensitive to the geometrical undercooling, leading to a high risk of SG defects. To produce the SC blade castings, the blade wax patterns with grain selectors at the bottom were assembled into a cluster (Figure 2a). Using the wax cluster, the shell molds were produced in a standard investment casting process. After the desired thickness was attained, the shell molds were de-waxed and subsequently sintered for the casting process (Figure 2b).

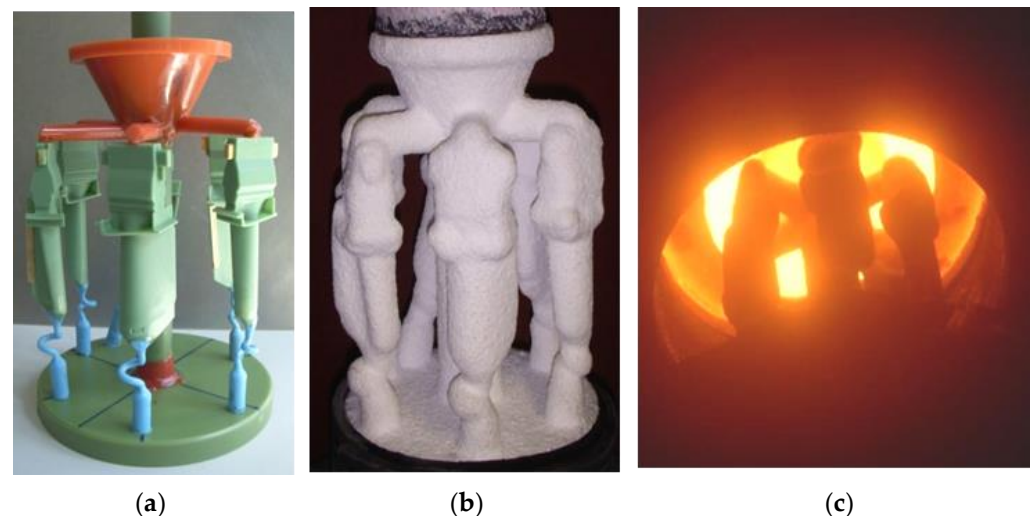


Figure 2. (a) Wax pattern cluster; (b) shell mold cluster; (c) withdrawal of poured mold in Bridgman furnace.

In an industrial Bridgman-type vacuum furnace, the shell mold placed on the chill plate was preheated in the heating chamber. After pouring the melt of a superalloy, the shell mold was withdrawn downward from the heating chamber to the cold chamber (Figure 2c). After the casting experiment for each superalloy listed in Table 1, the blade castings in the shell mold were knocked out and cut off from the casting cluster. After sand blasting and macro-etching, the blade castings were inspected for SGs, especially in the platform regions, to analyze the SC castability of the investigated alloys.

3. Results and Analysis

3.1. Evaluation of Undercooling Capacity

The undercooling capacity of an alloy reflects the tolerated undercooling ability of its melt before solidification begins. It could be evaluated by averaging the nucleation

undercooling values (ΔT_N) that were measured through the undercooling experiments. The temperature evolution of the PWA1483 samples during the cooling–heating cycles (Cycle 1 and Cycle 2) is compared to the heater temperature in Figure 3. The measured data were used to evaluate the characteristic temperatures of the investigated alloys, such as the nucleation temperature and the liquidus temperature.

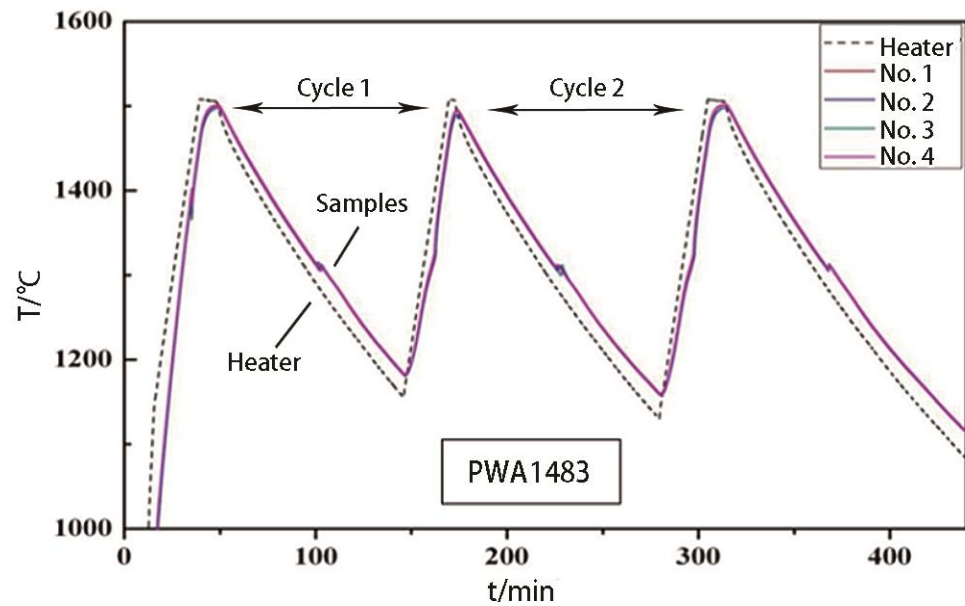


Figure 3. The measured temperature curves of the heater and four PWA1483 samples (No. 1 to No. 4) in the undercooling experiment.

The temperature evolution of the four CMSX-6 samples in the first cooling–heating cycle is illustrated in Figure 4. During the cooling stage, the measured curves for the four samples exhibit a clear temperature jump close to 1300 °C, which should be caused by the release of latent heat due to the triggering of the sample’s solidification. The lowest point on the cooling curve before recalescence, T_N , is the nucleation temperature of the alloy.

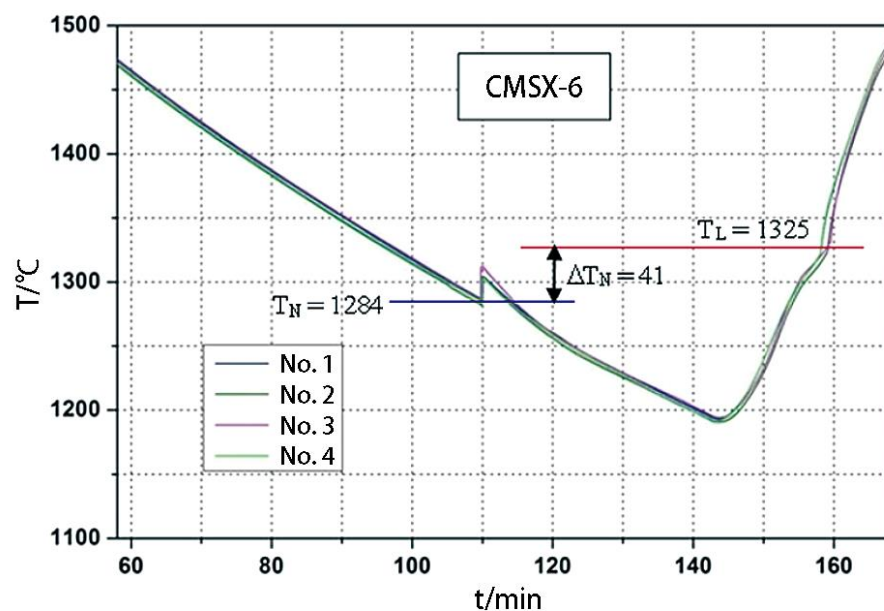


Figure 4. Temperature curves of the four samples of alloy CMSX-6 (No. 1 to No. 4), recorded in the first cooling–heating cycle. This figure serves to illustrate the approach to evaluating the characteristic temperatures T_N , T_L and ΔT_N .

When the temperature dropped below 1200 °C, the heaters were switched on again, leading to an increase in the measured temperature, as shown in Figure 4, i.e., the sample was reheated. In the early stage of the reheating process, the relatively slow heating rates were due to the absorption of the latent heat during the remelting of the solid phase. From 1325 °C, the heating rates of the samples increased obviously, which indicated that the solid phase was completely remelted. The corresponding temperature at this changing point was the liquidus temperature or melting point of the investigated superalloy (T_L). The difference between T_L and T_N , i.e., $\Delta T_N = T_L - T_N$, is the critical nucleation undercooling of the alloy. According to the cooling–heating curves, the T_N and T_L values of the CMSX-6 samples are equal to 1284 °C and 1325 °C, respectively, leading to the result of $\Delta T_N = 41$ K.

The temperature evolution of the DD483 samples during the first cooling–heating cycle is illustrated in Figure 5. In the same way, the liquidus temperature T_L and the nucleation temperature T_N were measured to be 1322 °C and 1313 °C, respectively. The nucleation undercooling was correspondingly evaluated to be 9 K, i.e., $\Delta T_N = 1322 - 1313 = 9$ K.

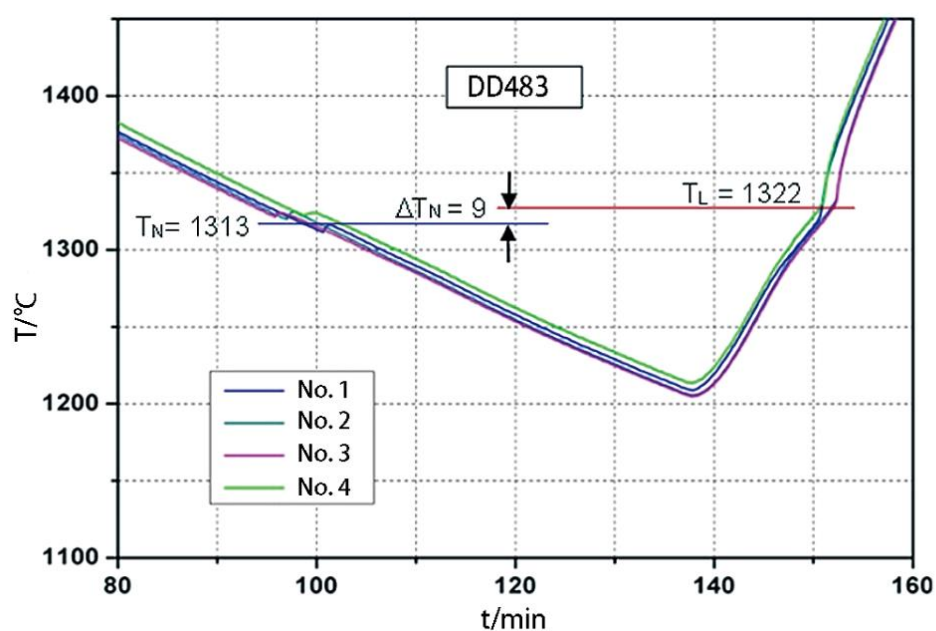


Figure 5. Temperature evolution of four DD483 samples (No. 1 to No. 4) recorded during the first cooling–heating cycle.

The experimental data of all alloy samples are summarized in Table 2. It is interesting to find that the Ni-based superalloys have significantly different undercooling capacity values, despite the same matrix element Ni and similar alloying elements. According to the measured undercooling capacity values listed in Table 2, the Ni-based superalloys are categorized into three groups: (1) highly uncontrollable alloys having ΔT_N values over 40 K, such as CMSX-6 and WZ30; (2) the alloys with medium ΔT_N values between 20 and 30 K, such as DZ445, MAR M247, CMSX-4 and PWA1483; (3) the alloys with very low ΔT_N values of around 10 K, such as IN939 and DD483. It is not clear why the alloy composition influences the undercooling capacity of the superalloys so strongly.

For each superalloy studied in this work, the total percentage of the added alloying elements ($\sum C_i$) was calculated and summarized, as in Table 1. Comparing the $\sum C_i$ values and ΔT_N values in Tables 1 and 2, CMSX-6 and WZ30 are the alloys having the lowest $\sum C_i$ values and the highest ΔT_N values. In contrast, the IN939 alloy has the highest addition of alloying elements ($\sum C_i = 50.4\%$), whose undercooling capacity is almost the lowest ($\Delta T_N = 10$ K). It appears that the alloys with a smaller addition of alloying elements ($\sum C_i$) exhibit a higher undercooling capacity (ΔT_N). In other words, the ΔT_N values of the superalloys tend to decrease with the $\sum C_i$ values; see Figure 6. There are also exceptions, e.g., the alloy DD483 shows high values for both $\sum C_i$ and ΔT_N . Therefore,

further investigation of the individual contribution of each alloying element is necessary to better understand the influence of the alloy composition on the undercooling capacity and its relationship with the formation of SG defects.

Table 2. The characteristic temperatures of the investigated superalloys, measured in the undercooling experiments.

Alloy	Liquidus Temperature T_L (°C)	Nucleation Temperature T_N (°C)	Nucleation Undercooling $\Delta T_N = T_L - T_N$ (K)	Undercooling Capacity Level
WZ30	1416	1374	42	High
CMSX-6	1325	1284	41	
DZ445	1347	1318	29	Medium
MAR M247	1368	1343	25	
CMSX-4	1372	1350	22	
PWA1483	1328	1307	21	
IN 939	1326	1316	10	Low
DD483	1322	1313	9	

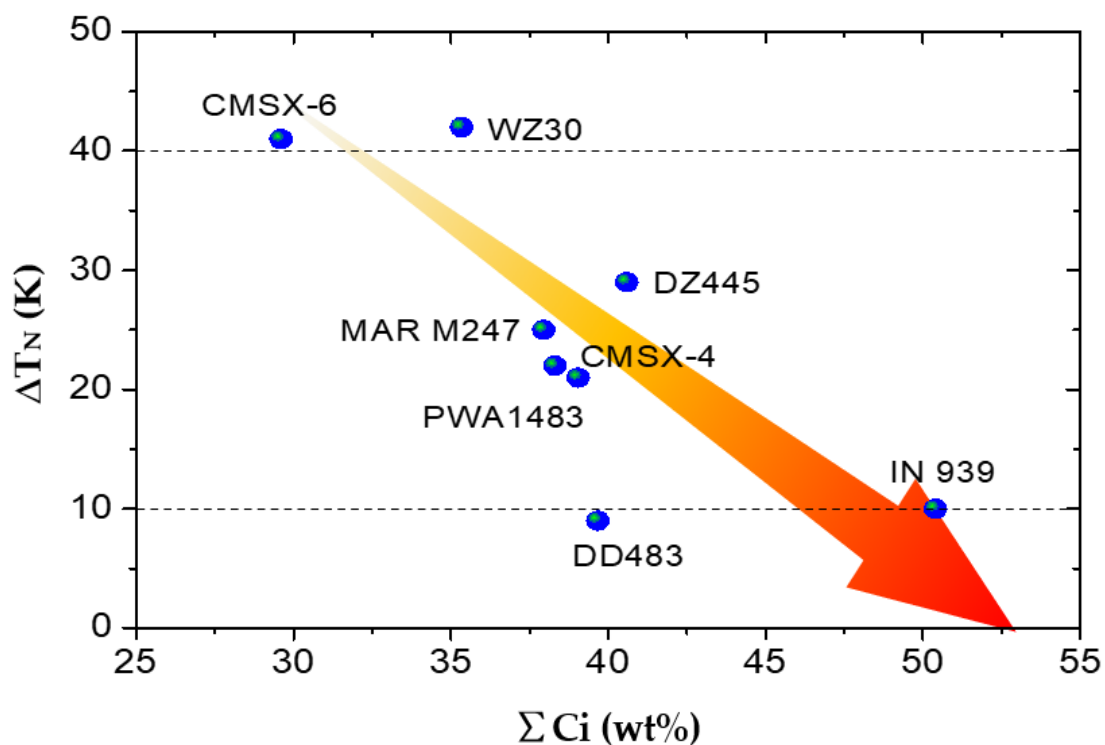


Figure 6. Influence of the total percentage of the added alloying elements (ΣC_i) on the undercooling capacity (ΔT_N) of the studied superalloys.

3.2. Inspection of Stray Grains in Blade Castings

Figure 7a shows a typical photo of the etched SC blades of alloy PWA 1483, in which no stray grains were found. Even the sensitive extremities of the blade platforms (Figure 7b), where the geometrical undercooling was the most serious, are also free of stray grains. In fact, all blades of this alloy have a single-crystal structure without SG defects. Besides PWA1483, the other alloys with medium undercooling capacity, as listed in Table 1, such as DZ445, MAR M247 and CMSX-4, exhibit also excellent castability for single crystals. Using this type of alloy, similar SG-free blades, as shown in Figure 7a, could be easily produced.

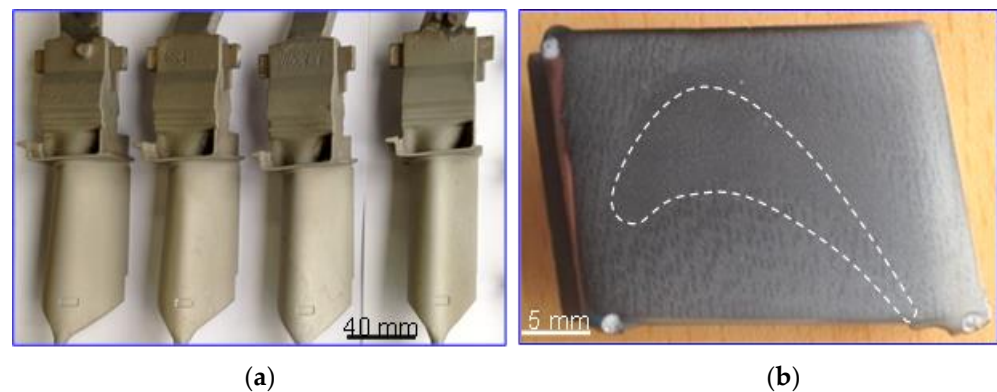


Figure 7. Casting results of the PWA1483 alloy. (a) Etched blade castings; (b) the corresponding platform, revealing SG-free structure.

Figure 8 presents the etched blade castings made from the alloy DD483, whose undercooling capacity is only 9 K (Table 2). In the blade root regions, as shown in Figure 8b, the SGs in the platform can be clearly distinguished from the SC matrix in the aerofoil region. As summarized in Table 2, the alloy DD483 has such a low ΔT_N value that it could be easily exceeded by the geometrical undercooling established at the extremities of the blade platforms, where the undercooling of the melt is up to dozens of degrees. The consequence is the nucleation of SGs at the platform extremities. The SGs will further grow into the blade roots in the subsequent solidification process. Another alloy in the low undercooling capacity group, the IN939 alloy (around 10 K in Table 2), is also shown to be SG-prone, and a similar structure to the results in Figure 7 was produced.

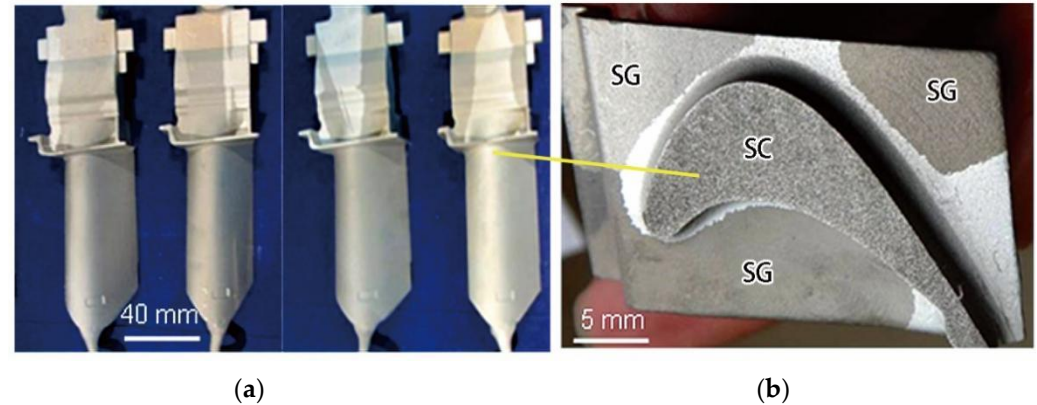


Figure 8. Casting results of the DD483 alloy. (a) Etched blade castings; (b) the SC growth in the airfoils and SGs originating from the platform extremities.

For CMSX-6 and WZ30, with a high undercooling capacity of over 40 K (Table 2), the SC structure of the blade castings could be achieved. Based on the current experimental study, no SGs were observed on the surface of the blade casting; see Figure 9a. However, in a microscopic inspection of the platform extremities, the fragmentation of the secondary dendrite arms was observed beneath the casting surface; see Figure 9b. In this case, the so-called SC microstructure is polycrystalline in reality, although no macroscopic grain boundaries can be detected on the casting surface. Due to the small size of the as-formed fragments, these microscopic structure defects are usually tolerated in the production of SC blade castings.

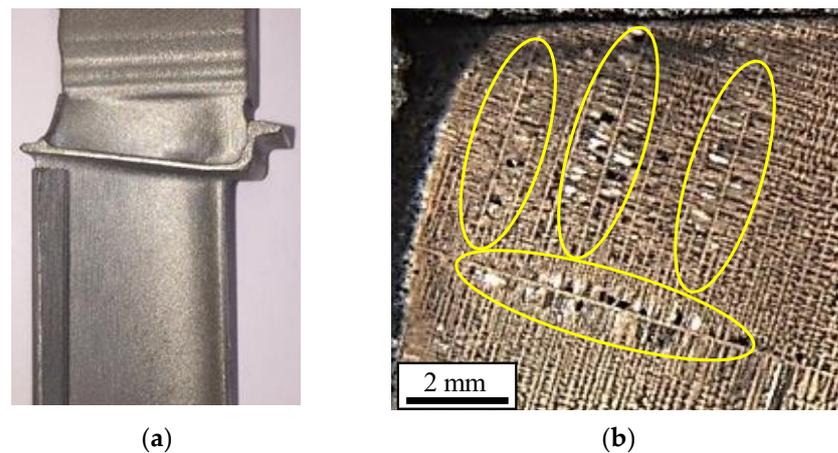


Figure 9. (a) Typical photo of the etched CMSX-6 blade, and (b) the cross-section of the platform extremity showing fragmentation of dendrite arms.

3.3. Analysis of Formation Mechanism of SG

As depicted schematically in Figure 10a, the currently used Bridgman furnace has a cylindrical configuration, including the heater on the top and the cooler on the bottom. The shell mold clusters are correspondingly arranged in a circle construction. During the directional solidification of blade castings by withdrawing the filled mold, SGs are often formed in the platforms with abrupt expansion, as indicated by the blue frame in Figure 10a and its magnified view in Figure 10b. Besides the undercooling capacity of the superalloy (alloy properties), the tendency to form SG defects can be influenced by other factors, such as the geometry expansion (geometrical effects) and the inclination of the liquidus isotherm in the platform regions (solidification conditions).

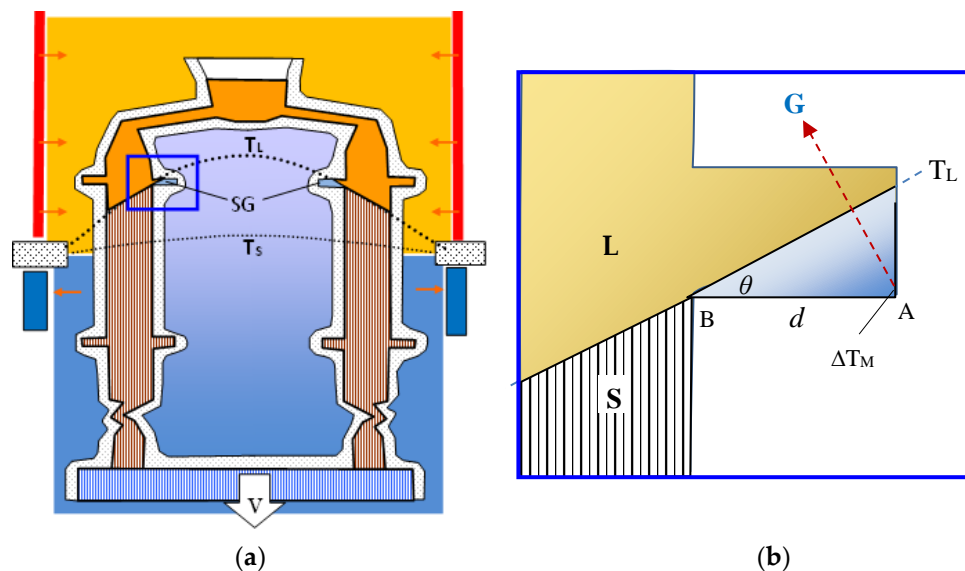


Figure 10. (a) Schematic to show the solidification process of blade castings during the withdrawal process in the Bridgman furnace; (b) magnified view of the blue frame area in (a) to illustrate the geometrical undercooling at a platform extremity. (T_L : liquidus temperature, θ : inclination angle, G : temperature gradient, ΔT_M : maximum undercooling, d : expansion distance).

In order to analyze the formation mechanism of the geometry-related SGs, a simplified platform with an expansion distance d is developed, as shown in Figure 10b. The liquidus isotherm T_L is simplified to an oblique line with an inclination angle θ . During the withdrawal process, the melt at corner A cools down much faster than the melt at corner B. After the T_L isotherm passes corner A (extremity), due to the geometrical effect of the

casting, the melt in the platform starts to be undercooled from corner A to the interior of the casting. When the T_L isotherm reaches corner B, the undercooling of the melt at corner A, i.e., $\Delta T_A = T - T_A$, reaches its maximum ΔT_M . This value can be calculated as the product of the expansion d and the lateral component of the local temperature gradient G :

$$\Delta T_M = d \times G \times \sin(\theta) \quad (1)$$

When ΔT_M exceeds ΔT_N , the nucleation of new grains seems to be unavoidable. Thus, an index F is proposed to quantify the formation potential of SGs as the ratio of the maximum undercooling (ΔT_M) at the extremity to the undercooling capacity (ΔT_N) of the alloy:

$$F = \frac{\Delta T_M}{\Delta T_N} = \frac{d \times G \times \sin(\theta)}{\Delta T_N} \quad (2)$$

A higher F value means higher potential for SG formation. The criterion for SG formation is then proposed as $F > 1$.

The three most important factors for the SG formation, i.e., casting geometry (d), solidification condition (θ), and alloy property (ΔT_N), are all included in the currently proposed index F , which can be reasonably used to predict and hence to control the formation of geometry-related SG defects. According to the F index criterion, a relatively flat T_L isotherm with a small angle θ should be established, so the probability for SG formation can be reduced. The blades in the cluster should be well arranged to keep the expansion d as short as possible. If the expansion d is extremely large, a grain continuator can be used as a bypass to transfer the SC growth to the extremities of the blade platforms [2,22]. In this case, the abrupt expansion distance d decreases to 0, and then the F index becomes 0, so that SG-free SC castings can be expected. However, during the withdrawal process, the growth direction of the dendrites in the grain continuator may deviate from the growth direction of the dendrites in the blade body. In this case, the formation of subgrain boundaries becomes inevitable.

As shown in Formula (2), the F index is inversely proportional to the undercooling capacity ΔT_N of the alloys. The alloys with a very low ΔT_N (e.g., DD483 and IN939) should have a very high probability to form SGs. This has been evidenced in this experimental work, as shown in Figure 8. In contrast, for the alloys with a medium or high ΔT_N (e.g., PWA1483 and CMSX-6), the SC blade castings should be easily produced. This has been also proven by the current experimental results, listed in Figures 7 and 9, respectively. However, we should mention that although the formation of macroscopic SGs on the casting surface can be eliminated, some small mis-oriented fragments (by pinching off the high-order side arms) may be produced in highly undercooled platform extremities; see Figure 9b. Based on the current study, the formation of SGs is highly related to the undercooling capacity of the superalloy. In order to reduce or even eliminate the geometry-related SG defects, a superalloy with a proper undercooling capacity (Table 2) should be used for the production of SC castings.

4. Conclusions

According to the experimental results regarding the undercooling measurements and SC castability, the currently studied Ni-based superalloys can be categorized into three groups:

1. Highly undercoolable alloys having an undercooling capacity of over 40 K. Using this type of alloy, SC blades without macroscopic SG defects could be produced easily. However, the occurrence of dendrite fragmentation in the platforms due to the locally high undercooling may result in microscopic defects.
2. The alloys having medium undercooling capacity between 20 and 30 K. The alloys with this moderate undercooling capacity exhibit optimal castability for SC blade castings. Both the macroscopic SG defects and the microscopic fragmentation of dendrite arms can be avoided.

- The alloys having very low undercooling capacity of only around 10 K. The undercooling capacity for these alloys is so low that it is normally exceeded by the geometrical undercooling established at the platform extremities, so these alloys are prone to the formation of SGs. It is very difficult to produce SC components free of SGs using this type of alloy.

Based on the experimental results, an analytical criterion to predict the occurrence of geometry-related SGs was proposed. The influences of three factors, i.e., the alloy property, casting geometry, and solidification condition, on the formation of SG defects are taken into account.

Author Contributions: Writing—original draft, Project administration, Conceptualization, D.M.; Methodology, Investigation, Y.Z.; Methodology, Formal analysis, W.X.; Formal analysis, Validation, F.X.; Resources, Supervision, J.W.; Writing—review & editing, H.Z. All authors have read and agreed to the published version of the manuscript.

Funding: This research was funded by the Shenzhen Peacock Plan (KQTD2015032716463668) and by the Guangdong Innovative and Entrepreneurial Research Team Program (607264877417).

Institutional Review Board Statement: Not applicable.

Informed Consent Statement: Not applicable.

Data Availability Statement: Not applicable.

Conflicts of Interest: The authors declare no conflict of interest.

References

- Pollock, T.; Murphy, W. The breakdown of single-crystal solidification in high refractory nickel-base alloys. *Metall. Trans. A* **1996**, *27*, 1081–1094. [[CrossRef](#)]
- Ma, D.; Wang, F.; Wu, Q.; Bogner, S.; Bührig-Polaczek, A. Innovations in casting techniques for single crystal turbine blades of superalloys. In *Superalloys*; Hardy, M., Huron, E., Glatzel, U., Griffin, B., Lewis, B., Rae, C., Seetharaman, V., Tin, S., Eds.; TMS: Warrendale, PA, USA, 2016; pp. 237–246.
- Wagner, A.; Shollock, B.A.; McLean, M. Grain structure development in directional solidification of nickel-base superalloys. *Mater. Sci. Eng. A* **2004**, *374*, 270–279. [[CrossRef](#)]
- Vehn, M.; Dedecke, D.; Paul, U.; Sahm, P.R. Undercooling related casting defects in SC turbine blades. In Proceedings of the International Symposium on Superalloys, Champion, PA, USA, 22–26 September 1996; pp. 471–479.
- Zhou, Y. Formation of stray grains during directional solidification of a nickel-based superalloy. *Scr. Mater.* **2011**, *65*, 281–284. [[CrossRef](#)]
- Bogner, S.; Ivanova, E.; Müller, M.; Wang, F.; Ma, D.; Bührig-Polaczek, A. Investigation of the undercoolability of Ni-Based alloys using high temperature thermal analysis. *Metals* **2015**, *5*, 1971–1983. [[CrossRef](#)]
- Yang, X.L.; Dong, H.B.; Wang, W. Microscale simulation of stray grain formation in investment cast turbine blades. *Mater. Sci. Eng. A* **2004**, *386*, 129–139. [[CrossRef](#)]
- Xuan, W.; Ren, Z.; Liu, H. Formation of stray grains in directionally solidified Ni-based superalloys with cross-section change regions. *Mater. Sci. Forum* **2013**, *747–748*, 535–539. [[CrossRef](#)]
- Xuan, W.; Ren, Z.; Li, C.; Ren, W.; Chen, C. Formation of stray grain in cross section area for Ni-based superalloy during directional solidification. *IOP Conf. Ser. Mater. Sci. Eng.* **2011**, *27*, 012035. [[CrossRef](#)]
- Zhang, J.; Huang, T.; Liu, L.; Hu, F. Advances in solidification characteristics and typical casting defects in nickel-based single crystal superalloys. *Acta Metall. Sin.* **2015**, *51*, 1163–1178.
- Xuan, W.; Ren, Z.; Li, C. Experimental evidence of the effect of a high magnetic field on the stray grains formation in cross-section change region for Ni-based superalloy during directional solidification. *Metall. Mater. Trans. A* **2015**, *46*, 1461–1466. [[CrossRef](#)]
- Paul, U.; Sahm, P.; Goldschmidt, D. Inhomogeneities in single-crystal components. *Mat. Sci. Eng. A* **1993**, *173*, 49–54. [[CrossRef](#)]
- Ma, D.; Wang, F.; Wu, Q.; Guo, J.; Xu, F.; Liu, Z.; Ou, S. Temperature evolution and grain defect formation during single crystal solidification of a blade cluster. *China Foundry* **2017**, *14*, 456–460. [[CrossRef](#)]
- Wang, F.; Wu, Z.; Huang, C.; Ma, D.; Bührig-Polaczek, A. Three-dimensional dendrite growth within the shrouds of single crystal blades of a nickel-based superalloy. *Metall. Mater. Trans. A* **2017**, *48*, 5924–5939. [[CrossRef](#)]
- Ma, D.; Bührig-Polaczek, A. Development of heat-conductor technique for single crystal components of superalloys. *Int. J. Cast Met. Res.* **2009**, *22*, 422–429. [[CrossRef](#)]
- Ma, D.; Bührig-Polaczek, A. Application of heat-conductor technique to production of single crystal turbine blade. *Metall. Mater. Trans. B* **2009**, *40*, 738–748. [[CrossRef](#)]

17. Xuan, W.D.; Zhang, H.W.; Shao, W.; Ren, Z. Formation Mechanism of stray grain of nickel-based single-crystal superalloy under a high magnetic field during directional solidification. *Metall. Mater. Trans. B* **2019**, *50*, 27–31. [[CrossRef](#)]
18. Li, Y.F.; Liu, L.; Sun, D.J.; Hu, F. Quantitative analysis of withdrawal rate on stray grain formation in the platforms of a Ni-Based single crystal dummy blade. *J. Alloy. Compd.* **2019**, *773*, 432–442. [[CrossRef](#)]
19. Qiu, F.; Bu, K.; Zheng, B.; Tian, G. Control of edge plate stray grain of single-crystal turbine blade by using process bar method. *Int. J. Met.* **2020**, *14*, 144–154. [[CrossRef](#)]
20. Yang, Z.Y.; Liu, C.G.; Hu, S.S.; Zheng, S.J.; Luo, Y.S.; Dai, S.L. Influence of platform position on stray grain nucleation in Ni-based single-crystal dummy blade clusters. *China Foundry* **2021**, *18*, 442–449. [[CrossRef](#)]
21. Ma, D.; Wu, Q.; Bührig-Polaczek, A. Undercoolability of Superalloys and Solidification Defects in Single Crystal Components. *Adv. Mat. Res.* **2011**, *278*, 417–422. [[CrossRef](#)]
22. Ma, D. Novel casting processes for single crystal turbine blades of superalloys. *Front. Mech. Eng.* **2018**, *13*, 3–16. [[CrossRef](#)]
23. Ma, D.; Wang, F.; Guo, J.; Xu, W. Single Crystal Castability and Undercoolability of PWA1483 Superalloy. *Acta Metall. Sin.* **2019**, *32*, 1415–1420. [[CrossRef](#)]

Disclaimer/Publisher’s Note: The statements, opinions and data contained in all publications are solely those of the individual author(s) and contributor(s) and not of MDPI and/or the editor(s). MDPI and/or the editor(s) disclaim responsibility for any injury to people or property resulting from any ideas, methods, instructions or products referred to in the content.